

Frequency-Domain Characterization of Load Demand from Electrified Highways

Ashutossh Gupta, *Student Member, IEEE*, Vassilis Kekatos, *Senior Member, IEEE*, Ruoyu Yang, *Student Member, IEEE*, Dionysios Aliprantis, *Fellow, IEEE*, and Steve Pekarek, *Fellow, IEEE*

Abstract—Electrified roadways (ER) equipped with dynamic wireless power transfer (DWPT) capabilities can patently extend the driving range and reduce the battery size of electric vehicles (EVs). However, due to the spatial arrangement of the transmitter coils in the ER, the DWPT load exhibits frequency content that could excite power system frequency dynamics. In this context, this work aims to study the spectrum of DWPT loads under different traffic conditions. We develop statistical models for EVs moving at constant speeds to identify the location and magnitude of DWPT load harmonics. Our analysis reveals that the fundamental frequency is dependent on the ER coil spacing and the average EV speed. In the worst-case yet unlikely scenario that EVs move in a synchronized fashion, the amplitude of harmonics scales with the number of EVs. On the contrary, when EVs move freely, harmonics scale with the square root of the number of EVs. Platoon formations can accentuate harmonics. We also show that for higher-order harmonics, the spectral content around harmonics decreases in magnitude and increases in bandwidth. Despite the simplified models, our analysis offers valuable insights for ER planners and grid operators. Numerical tests using a traffic simulator corroborate some of these insights.

Index Terms—EV charging, oscillations, power spectra, power system dynamics, statistical analysis.

I. INTRODUCTION

Electrified roadways (ERs) with DWPT capabilities have been proposed to power EVs during transit. The power can be used directly for vehicle propulsion and to charge a battery if needed. DWPT-enabled ERs are expected to offer multiple benefits, such as extended EV range, reduced battery size, and reduced overall battery charging time [1]. DWPT systems may also contribute to increasing EV adoption along with potential cost benefits [2]. From a power grid perspective, with growing EV penetration, stationary EV charging is expected to increase the load on distribution systems significantly [3]. For instance, reference [4] shows that even if 11% of the total number of heavy-duty EVs in Texas charge simultaneously, they would create significant voltage violations. While stationary EV charging loads are concentrated at specific grid buses, DWPT-enabled ERs can distribute EV load across multiple buses.

The DWPT system relies on an array of transmitters (Tx) embedded in the ER that supply power to receivers (Rx) installed on EVs. Successive Tx coils on the ER are separated by a gap [5]. Owing to the spatial arrangement of the Tx coils, the power consumed by each EV exhibits a time-varying, near-periodic waveform. A segment of an ER draws power from the power grid through a substation. The load at the substation equals the total power drawn by all EVs while driving on this ER segment, plus losses. This work aims at modeling the total DWPT load consumed at this substation in the frequency domain.

Previous works predict the average amount of power consumed by the ER infrastructure [6]. Such DWPT load predictions are crucial for system operators to conduct unit commitment, economic dispatch, and power flow studies, as well as determine market prices [7]. Using similar DWPT load predictions, researchers have also designed battery storage systems and control mechanisms to regulate voltage on the distribution grid feeding the ER [8]. Reference [9] studies the optimal location of DWPT lanes, and [10] investigates the vehicle-to-grid power transfer capabilities during blackouts.

While hourly-averaged load profiles of DWPT loads are essential for grid scheduling, they cannot predict the impact of ERs on power grid frequency dynamics. Because stationary EV loads are approximately constant over finer time scales, they have not been a concern for exciting power system oscillations. On the contrary, dynamic EV loads are time-varying and thus pose the risk of introducing oscillations into the power grid. To model the dynamic impact of a DWPT system, its load demand needs to be studied at the timescale of seconds. By assessing the shape of the DWPT frequency spectrum, grid operators can evaluate whether ERs could introduce frequency oscillations into transmission systems.

Transmission system operators are generally interested in identifying possible sources of sustained low-frequency oscillations, also known as *inter-area oscillations* [11]. These oscillations generally occur at frequencies below 2 Hz and can lead to widespread blackouts if not properly damped; see the recent 2025 Iberian Peninsula blackout [12]. Such oscillations can be triggered due to malfunctions in switching of power electronic devices [13], [14]; sudden loss of load and generators [15]; as well as pulsating electrical loads [16]. Identifying the sources of these oscillations based on real-time measurements is time-intensive. Therefore, it becomes pertinent for power system operators to pre-identify potential sources of such oscillations. This work aims to develop models that determine the frequency spectrum of the total power consumed by a DWPT system under various traffic conditions. Such models are helpful for grid operators and ER designers to understand the impact of DWPT systems on power system dynamics and develop appropriate solutions.

Studies have attempted to predict the real-time power consumption by an ER under diverse traffic flow conditions [17], [18]. However, they have not considered the effect of Tx coil segmentation. Reference [1] incorporated the effect of coil segmentation in determining DWPT load demand under different EV penetration levels. Nonetheless, the DWPT spectrum was computed numerically and averaged over diverse traffic conditions, as the time gap between successive EVs was drawn from a distribution inferred based on year-long

traffic flow data. Recent work [19] proposes a discrete-time convolution-based method to ascertain the power consumed by DWPT systems, but the analysis does not consider the stochastic nature of traffic.

This work contributes to the ensuing fronts:

- c1) We develop statistical models for the DWPT load consumed at a substation serving an ER segment (Section II). The DWPT load is modeled as a continuous-time signal and analyzed in the time and frequency domains. Based on these models, we identify the location and amplitude of frequency harmonics of the DWPT load and study its *total harmonic content* (THC), defined as the ratio between the non-DC and DC components. Our analysis establishes scaling laws to inform ER designers and grid operators about the potential impact of DWPT loads on grid frequency dynamics.
- c2) Our findings on the DWPT spectrum are summarized as follows (Sec. III–IV):
 - Depending on the ER coil spacing and EV speed, the DWPT load can exhibit frequency content below 2 Hz, that is, within the range of inter-area oscillations.
 - Assuming vehicles move at a common and constant speed, the highest THC occurs when EVs move in a synchronized fashion. In this worst-case yet unlikely scenario, both the average (DC) DWPT load and its harmonics scale with the number of EVs N .
 - When EVs move asynchronously, harmonics do not disappear, but scale with \sqrt{N} .
 - Between the two previous extremes, an intermediate case occurs when EVs form platoons with Q EVs per platoon. In this case, harmonics scale with \sqrt{QN} .
 - If EVs move at constant yet unequal speeds, the total DWPT load becomes non-periodic. Its spectrum consists of bells centered around harmonics of the average speed. Moreover, the bells decrease in magnitude and increase in bandwidth for higher harmonics.
- c3) Our findings are validated numerically in two ways:
 - Periodograms of randomly sampled DWPT loads resemble the analytically derived spectra (Section V).
 - DWPT loads generated by the SUMO traffic flow simulator demonstrate that free-moving traffic yields mild THC, whereas slower-speed, heavier traffic could lead to synchronization (Sec. VI).

II. TIME-DOMAIN MODEL OF DWPT LOAD DEMAND

This section models the total power consumed by all EVs powered by a DWPT-enabled ER. Hereafter, we will refer to DWPT-enabled EVs simply as EVs. Most existing DWPT studies propose installing the DWPT technology only on a single lane of a highway [18]. We thus assume that DWPT is offered on a single lane and consider one direction of the ER. We consider an ER segment of length L that is powered by a substation. We are interested in modeling the power demand at that substation in the time and frequency domains.

The ER consists of Tx coils, each of length ℓ_T , laid in a linear arrangement; see Fig. 1. Consecutive coils are spaced d meters apart due to road construction specifications. Each Tx

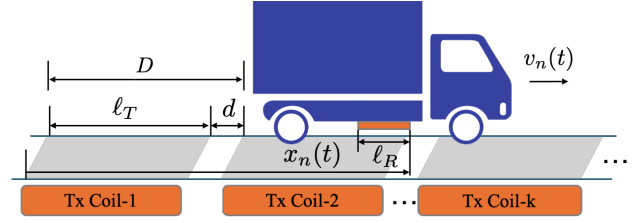


Fig. 1. In a DWPT-enabled ER, transmitters Tx of length ℓ_T and gaps of length d are arranged periodically, every $D = \ell_T + d$ meters. A DWPT-enabled EV draws power when its Rx of length ℓ_R overlaps with Tx coils.

coil and the subsequent gap d will be termed a *coil segment* of length

$$D = \ell_T + d. \quad (1)$$

The pattern of coil segments is repeated in the direction of traffic flow with period D . Coil segments are indexed by $k = 0, \dots, K-1$, where $K = L/D$. Electric vehicles are instrumented with Rx of length ℓ_R . Although our analysis assumes ℓ_R to be fixed across EVs, it can be extended to capture EVs of different types, and hence, different Rx lengths.

Suppose the ER segment serves N EVs, indexed by $n = 1, \dots, N$. We first model the power consumed by a single EV. The power consumed by the n -th EV, or simply EV_n , depends on two factors: *i*) The overlap of its Rx with the Tx coils, measured in meters; and *ii*) The spatial density a_n (in kW/m) of power absorbed by EV_n per meter of Rx/Tx overlap. Leaving a_n aside for now, let us focus on the Rx/Tx overlap as a function of the EV's position. In detail, if $\ell_T \geq \ell_R$, the overlap of the Rx with the first Tx coil can be computed as

$$O(x_n) = \begin{cases} x_n, & 0 \leq x_n < \ell_R \\ \ell_R, & \ell_R \leq x_n < \ell_T \\ \ell_R + \ell_T - x_n, & \ell_T \leq x_n < \ell_T + \ell_R \\ 0, & \text{otherwise,} \end{cases} \quad (2)$$

where x_n is the distance between the front end of the Rx for EV_n and the back end of the first Tx coil; see Fig. 1. Because coil segments are D meters long, the overlap of the Rx with the $(k-1)$ -th Tx coil is $O(x_n - kD)$ for $k = 0, \dots, K-1$. Then, the power demand of EV_n can be expressed as

$$\bar{p}_n(x_n) = a_n \sum_{k=0}^{K-1} O(x_n - kD). \quad (3)$$

Effects, such as Rx/Tx misalignment, voltage drops across the distribution system feeding the ER, and losses could be captured by adding noise terms in (3), but are ignored for simplicity. The model in (3) also neglects high-frequency harmonics due to the switching of power converters.

It is clear from (3) that the load of EV_n is a periodic function of the EV's position. Nevertheless, to analyze the DWPT load in the frequency domain, we need to model the load of EV_n across time rather than position. Let $x_n(t)$ be the position of EV_n at time t , and $v_n(t) = \dot{x}_n(t)$ be its speed. The load of EV_n can then be expressed as a function of time as

$$p_n(t) = \bar{p}_n(x_n(t)) = a_n \sum_{k=0}^{K-1} O(x_n(t) - kD). \quad (4)$$

Example 1. We will often refer to the *INDOT ER testbed*, a pilot project of an ER under development by the Indiana Department of Transportation (INDOT); see [5]. The rightmost lane out of two lanes is instrumented with DWPT technology for a stretch of 400 m with $\ell_T = 3.66$ m and $d = 0.91$ m. A prototype DWPT-enabled EV has also been developed, featuring an Rx of length $\ell_R = 1.8$ m. The speed limit is $v = 24.6$ m/s or 55 mph. This testbed is designed to provide up to 200 kW to an Rx of length $\ell_R = 1.8$ m, yielding a spatial power density of up to $\bar{a} = 111.11$ kW/m.

Regarding a_n , it is determined by the ER power rating and the EV controller. The ER comes with a rated density \bar{a} in kW/m. This is the maximum power an EV can extract from the ER per meter of Rx/Tx overlap; see blue waveform in Fig. 2. However, depending on the load demand, the EV controller may require less power. This can be implemented in different ways. One option would be to scale down the rated density so that the effective density is set to some $a_n \leq \bar{a}$ in kW/m; see green waveform in Fig. 2. The model in (4) captures this multiplicative option. Another option is for the EV controller to saturate its peak density to a value below \bar{a} ; see red waveform of Fig. 2. In this case, the load of EV_{*n*} is a *clipped* rather than a scaled version of the blue waveform. This clipping option simplifies the implementation of the EV controller and has been implemented on the EV prototype for the INDOT testbed. The model in (4) can capture clipping by adjusting the Rx/Tx overlap function per EV. To simplify the analysis, we will henceforth adopt the multiplicative option.

The total DWPT load demand at the substation serving this ER segment is the sum of EV loads:

$$p(t) = \sum_{n=1}^N p_n(t). \quad (5)$$

We are interested in assessing the frequency spectrum of $p(t)$. A key challenge to doing so is that EV positions, speeds, and densities can be random and time-varying. To this end, we postulate statistical models for $p(t)$ to account for various traffic conditions and derive the corresponding spectra. We study four models or scenarios:

- S1) EVs move at a common constant speed and synchronize in time so their load waveforms add constructively. Although such perfect synchronization is unlikely to occur, it serves as a worst-case scenario.
- S2) EVs move at a common constant speed and are randomly spaced apart.
- S3) EVs move at a common constant speed and form platoons.
- S4) EVs move at different constant speeds and are randomly spaced apart.

III. EVs MOVING AT COMMON CONSTANT SPEEDS

In this section, we study the spectrum of the DWPT load under the first three scenarios. These scenarios assume that all EVs move at a common and constant speed, that is $v_n(t) = v$ for all n and t . This assumption simplifies the analysis and

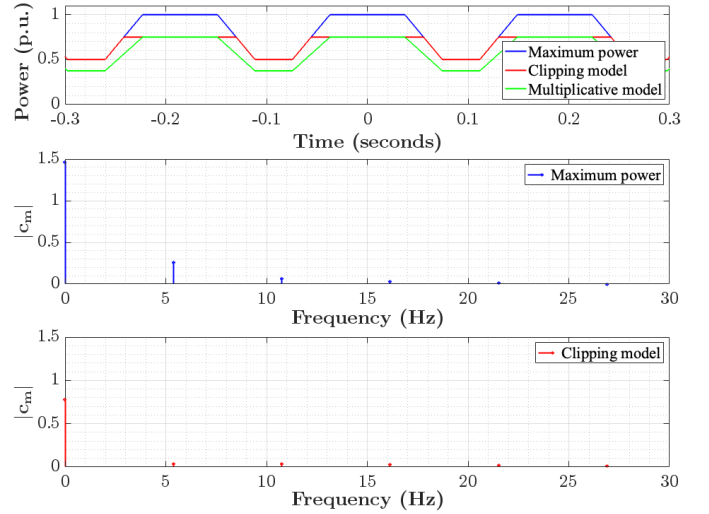


Fig. 2. DWPT load $p_n(t)$ (top) for an EV with Rx length $\ell_R = 1.8$ m moving at $v = 24.65$ m/s (55 mph) on the INDOT ER testbed. Blue and green EV loads occur when the EV controller follows the multiplicative model with $a_n = \bar{a}$ and $a_n = 0.75\bar{a}$, respectively. The red EV load occurs when the EV controller clips the power it draws at $0.75\bar{a}$. Because $\ell_R > d$, the load is strictly positive at all times. The FS line spectra of blue (middle) and red (bottom) waveforms are also shown. Both spectra peak at harmonics mf_0 with $f_0 = 5.38$ Hz.

offers valuable insights. Under constant speed, the position of EV_{*n*} at time t can be expressed as

$$x_n(t) = v \cdot (t - t_n) \quad \text{for } t \geq t_n, \quad (6)$$

where t_n is the time EV_{*n*} moves over the first Tx coil, and will be termed as the *timing* of EV_{*n*}. When EV_{*n*} moves at a constant speed, its power demand is periodic in time. Precisely, substituting (6) into (4) yields

$$p_n(t) = a_n \sum_{k=0}^{K-1} O(v \cdot (t - t_n - kT)), \quad (7)$$

where $T = D/v$ is the *fundamental period* of $p_n(t)$. It is clear from (7) that each $p_n(t)$ is a scaled and time-shifted version of the periodic signal

$$h_T(t) = \sum_{k=-\infty}^{\infty} O(v \cdot (t - kT)). \quad (8)$$

The signal $h_T(t)$ is a train of trapezoidal pulses of period T ; it is a scaled version of the blue waveform shown in Fig. 2. Although $h_T(t)$ has infinite duration, it is a good approximation of the finite-duration signal $p_n(t)$ because the number of coil segments K is large. The signal $h_T(t)$ has been time-shifted so it is even symmetric around $t = 0$.

Given that $h_T(t)$ is periodic, it is amenable to the Fourier series (FS) expansion

$$h_T(t) = \sum_{m=-\infty}^{\infty} c_m e^{jm\omega_0 t}, \quad (9)$$

where $\omega_0 = 2\pi/T = 2\pi v/D$ is the fundamental frequency and c_m is the FS coefficient related to the m -th harmonic.

Given that $h_T(t)$ is real-valued and even-symmetric, the FS coefficients are real-valued and even-symmetric (see Fig. 2):

$$c_m = \begin{cases} \frac{\ell_T \ell_R}{D}, & m = 0 \\ \frac{D}{m^2 \pi^2} \sin\left(m\pi \frac{\ell_R}{D}\right) \sin\left(m\pi \frac{\ell_T}{D}\right), & m \neq 0. \end{cases} \quad (10)$$

For the INDOT testbed, we get $c_5 = 0$ because $\ell_T/D = 4/5$.

Based on (7) and the time-shifting property of the FS, the FS expansion of $p_n(t)$ is

$$p_n(t) = a_n h_T(t - t_n) = a_n \sum_{m=-\infty}^{\infty} c_m e^{jm\omega_0 t} e^{-jm\omega_0 t_n}. \quad (11)$$

The timing t_n affects $p_n(t)$ through harmonic trigonometric functions with fundamental period T , and thus introduces a phase shift on the periodic signal $h_T(t)$. To simplify the presentation, we will henceforth slightly abuse notation and use t_n to denote the original timing of EV_n modulo T . Therefore, the timing $t_n \in [0, T)$ now captures the relative timing at which EV_n aligns with the pattern of Tx coils.

From (9)–(11), it is worth identifying the following properties of $h_T(t)$ and $p_n(t)$:

- p1) The fundamental frequency $\omega_0 = 2\pi v/D$ grows with the EV speed and the inverse of D . For the INDOT testbed, we get $f_0 = 5.38$ Hz for $v = 24.56$ m/s (55 mph), and f_0 falls below 2 Hz when $v < 9.83$ m/s (22 mph).
- p2) Although the locations of harmonics $m\omega_0$ depend on the EV speed, the FS coefficients c_m depend only on Rx/Tx dimensions. To capture the undesirable frequency content, we define the metric of *total harmonic content* as the ratio

$$\text{THC} = \frac{\sqrt{2 \sum_{m=1}^{\infty} |c_m|^2}}{c_0} \times 100\%. \quad (12)$$

For the INDOT testbed, signal $h_T(t)$ has $\text{THC}_h = 26\%$.

- p3) Only the first few harmonics contribute notably to $p_n(t)$. For the INDOT ER testbed, with $c_1 = 0.18c_0$, the first harmonic contributes 25.45% to the THC of 26%.

Having characterized the frequency content of $h_T(t)$ and $p_n(t)$, we shift focus to the DWPT load $p(t)$. Plugging (11) into (5) shows that $p(t)$ is also periodic:

$$p(t) = \sum_{n=1}^N p_n(t) = \sum_{m=-\infty}^{\infty} \tilde{c}_m e^{jm\omega_0 t} \quad (13)$$

with fundamental frequency $\omega_0 = 2\pi v/D$ and FS coefficients

$$\tilde{c}_m = c_m \sum_{n=1}^N a_n e^{-jm\omega_0 t_n}. \quad (14)$$

This leads to the next obvious, yet important, remark.

Remark 1. *Under constant EV speed, the DWPT load $p(t)$ can include frequency components below 2 Hz (that is, within the range of inter-area oscillations) if the EV speed v in m/s and the coil segment length D in m satisfy $v < 2D$.*

We next study the frequency content of the DWPT load under the first three traffic scenarios.

A. Scenario S1): Perfect Time Synchronization

According to (14), the FS coefficients \tilde{c}_m of $p(t)$ critically depend on EV timings. This subsection considers the worst-case scenario in terms of THC of $p(t)$. To build up some intuition, suppose EV densities are equal for now, that is, $a_n = a$ for all n . If EVs have equal timings, EVs drive over the coil segments in a synchronized fashion. In this case, EV loads $p_n(t)$ add up constructively, and the total load $p(t)$ becomes a time-shifted version of $Nah_T(t)$. Then, the total DWPT load inherits properties p1)–p3). For general EV densities a_n , the ensuing lemma identifies worst-case EV settings that maximize THC; all proofs are provided in the appendix.

Lemma 1. *Under the assumption of a common constant EV speed, the maximum THC is realized if EVs have equal timings $\{t_n\}_{n=1}^N$, regardless of the EV densities $\{a_n\}_{n=1}^N$. Then, the maximum THC for $p(t)$ coincides with the THC of $h_T(t)$. Equal timings also maximize the harmonic ratios $|\tilde{c}_m|/\tilde{c}_0$ for $m \geq 1$. If $a_n = a$ for all n , the Fourier transform of $p(t)$ is*

$$P(\omega) = 2\pi Na \sum_{m=-\infty}^{\infty} c_m \delta(\omega - m\omega_0),$$

where $\delta(\omega)$ is the Dirac delta function.

Lemma 1 suggests that if EVs move synchronously and their spacings align with the ER coil spacing, the DWPT load spectrum can have THC equal to that of $h_T(t)$, which is 26% for the INDOT testbed. Both the DC and harmonic components of $p(t)$ then scale with N . Moreover, as Remark 1 suggests, single-frequency components can occur in the 0–2 Hz range at slower EV speeds.

Admittedly, EVs are unlikely to be perfectly synchronized in practice. EVs may be approximately synchronized under heavy traffic conditions, when drivers may generally follow the *2-second rule*. According to this rule, a driver maintains a two-second spacing between their vehicle and the leading vehicle. If the distance $2v$ traveled in two seconds is an integer multiple of D , EVs can get synchronized. Holding S1) as a worst-case scenario, we next study some more realistic conditions.

B. Scenario S2): Independent Uniformly Distributed Timings

Given that individual EV loads can be rather arbitrary, any deterministic modeling of $\{p_n(t)\}_{n=1}^N$ may be of limited value. For a more systematic characterization of the DWPT load spectrum, we suggest treating these signals as stochastic. To find the frequency content of $p(t)$, one may apply the Fourier transform to $p(t)$. Unfortunately, the Fourier transform is undefined for stochastic signals. Instead, one may define the *power spectral density* (PSD) $S_p(\omega)$ of $p(t)$. The PSD describes how the power of a stochastic signal is distributed across frequencies. Note that the term *power* is used here in two contexts. The signal $p(t)$ denotes the electric power consumed by the ER and is measured in W (Watts), but we can also define the power of the signal $p(t)$, measured in W^2 .

A sufficient condition for the PSD of a stochastic signal to exist is that the signal is *wide sense stationary* (WSS) [20,

Ch. 4]. A stochastic signal $p(t)$ is WSS if its mean does not vary with time and its autocorrelation depends only on the lag:

$$\mathbb{E}[p(t)] = \mu_p, \quad \text{and} \quad \mathbb{E}[p(t)p(t+\tau)] = R_p(\tau), \quad \forall t.$$

If $p(t)$ is WSS, its PSD can be computed as the Fourier transform of its autocorrelation function as

$$S_p(\omega) = \mathcal{F}[R_p(\tau)]. \quad (15)$$

We next compute the PSD of $p(t)$ under different statistical models on EV parameters $\{(a_n, t_n)\}_{n=1}^N$.

Subsection III-A considered the worst-case scenario where EVs are perfectly synchronized. This subsection examines the opposite extreme of no synchronization between EVs. This scenario, termed *S2*), can occur when EVs are spaced sufficiently far apart and move freely. Under *S2*), we model EV timings t_n as independent and identically distributed (iid) random variables uniformly drawn from $[0, T)$. It is reasonable to assume that t_n is uniformly distributed through any time interval; we select the interval $[0, T)$ without loss of generality for mathematical convenience. We model EV densities a_n as independent and identically distributed (iid) random variables with a given mean and variance. It is reasonable to assume that EV densities are independent of EV timings.

As $p(t)$ is the sum of several randomly time-shifted replicas of $h_T(t)$, one may conjecture that $p(t)$ approaches a constant (time-invariant) signal as N grows, so its harmonics eventually disappear. The ensuing result sets the correct scaling law of DWPT harmonics.

Lemma 2. *Suppose EVs move at constant speed v ; EV densities a_n are iid with mean μ_a and variance σ_a^2 ; and EV timings t_n are iid uniformly within $[0, T)$. Then, the DWPT load $p(t)$ is WSS with mean $\mu_p(t) = N\mu_a c_0$ and PSD:*

$$S_p(\omega) = 2\pi(N^2\mu_a^2 + N\sigma_a^2)c_0^2\delta(\omega) + 2\pi N(\mu_a^2 + \sigma_a^2) \sum_{m \neq 0} c_m^2 \delta(\omega - m\omega_0).$$

According to Lemma 2, the spectrum of $p(t)$ under *S2*) contains the same harmonics as in *S1*). Recall that under *S1*), the DC term and harmonics of $p(t)$ scale with N . Under *S2*), harmonics do *not* disappear, but scale differently. To simplify the analysis, suppose $\sigma_a^2 = 0$ and $\mu_a = a$, so EV densities become deterministic and conform with Corollary 1. Then, Lemma 2 explains that the DC term under *S2*) scales with Nac_0 , whereas its m -th harmonic scales with $\sqrt{N}a|c_m|$. The key conclusion from this analysis is that even when EV timings are independent, DWPT harmonics do not disappear, but scale with \sqrt{N} rather than N .

C. Scenario *S3*): Vehicle Platoons

Vehicles driving on a highway often form *platoons*, i.e., groups of vehicles moving together at the same speed. This subsection studies the effect of EV platoons on the DWPT signal. Suppose the N EVs served by an ER segment form platoons. To ease the analysis under *S3*), we assume:

- i) each platoon has the same number of EVs, Q ;
- ii) EVs within a platoon are perfectly time-synchronized;

- iii) the timing for each platoon is iid and uniformly in $[0, T)$;
- iv) EV densities are iid of given mean μ_a and variance σ_a^2 .

Assumption *ii*) considers the worst-case scenario where EVs within a platoon move synchronized and at spacings that are integer multiples of D . Scenario *S3*) can be studied by combining *S1*) and *S2*). If EVs within a platoon get synchronized, they can be modeled as a single EV of a larger rating. On the other hand, timings across platoons can be modeled as independent and uniformly distributed. Based on these two points, we next derive the PSD of $p(t)$ under *S3*).

Lemma 3. *Under the assumptions of *S3*), the mean of $p(t)$ is $N\mu_a c_0$ and its PSD is*

$$S_p(\omega) = 2\pi(N^2\mu_a^2 + N\sigma_a^2)c_0^2\delta(\omega) + 2\pi N(Q\mu_a^2 + \sigma_a^2) \sum_{m \neq 0} c_m^2 \delta(\omega - m\omega_0).$$

To quantify the effect of platoon formations, compare Lemma 3 to Lemma 2. To ease the comparison, consider deterministic EV densities by setting $\sigma_a = 0$ and $\mu_a = a$. Although the DC component under *S3*) remains Nac_0 , harmonics scale now as $\sqrt{NQ}a|c_m|$ instead of $\sqrt{N}a|c_m|$. Clearly, harmonic components are more prominent in *S3*) compared to *S2*). This is expected as platoon formations imply less smoothing across time-shifted replicas of $h_T(t)$. Therefore, platoon formations can increase the THC in $p(t)$. When $Q = 1$, scenario *S3*) becomes equivalent to *S2*). On the other extreme, when $Q = N$, scenario *S3*) becomes *S1*).

Remark 2. *Our analysis assumes a constant number N of EVs on the ER segment. A more detailed analysis should model N as a random variable. Traffic flow studies usually postulate that EV arrivals follow a Poisson distribution parameterized by the mean arrival rate λ_a , measured in EV/s. If all EVs move at constant speed v , the total number N of EVs driving on an ER segment of length L follows a Poisson distribution with mean $\lambda_N = \lambda_a L/v$; see [21, Sec 8.3]. If $\lambda_a = 0.3$ EV/s, $L = 10$ mi, and $v = 55$ mph, we get the mean value of $\lambda_N = 192$. Moreover, the probability of N being within $\pm 10\%$ of its mean value $\lambda_N = 192$ is 84%. To simplify the analysis, we treat N as deterministic and set it to its mean value λ_N determined by (λ_a, L, v) .*

IV. EVS MOVING AT CONSTANT BUT UNEQUAL SPEEDS

We have hitherto assumed that EVs move at a common constant speed, resulting in the DWPT load $p(t)$ being periodic in time. This section considers the scenario where EVs move at constant yet unequal speeds. In this case, although each EV load $p_n(t)$ is periodic, the DWPT load $p(t)$ is non-periodic, and thus, has a continuous spectrum.

A. Scenario *S4*): Constant Gaussian-Distributed Speeds

Consider first a single EV. Similar to (11), if EV_n moves at constant speed v_n , its power demand $p_n(t)$ is periodic with fundamental period $T_n = D/v_n$ and fundamental frequency $\omega_n = 2\pi v_n/D$. Signal $p_n(t)$ has the FS expansion:

$$p_n(t) = a_n \sum_{m=-\infty}^{\infty} c_m e^{jm\omega_n(t-t_n)} \quad (16)$$

with the FS coefficients defined as in (10). EV densities a_n are again modeled as iid with mean μ_a and variance σ_a^2 . Different from Sec. III, here speeds v_n are modeled as iid Gaussian random variables distributed as $v_n \sim \mathcal{N}(\mu_v, \sigma_v^2)$. If v_n is Gaussian, the fundamental frequency $\omega_n = 2\pi v_n/D$ is also Gaussian with mean and variance:

$$\mu_\omega = \frac{2\pi\mu_v}{D} \quad \text{and} \quad \sigma_\omega^2 = \frac{4\pi^2\sigma_v^2}{D^2}.$$

Regarding EV timings t_n , it is reasonable to assume they are uniformly distributed in $[0, T_n)$. Parameters (a_n, v_n, t_n) are assumed to be independent across EVs.

Under S4), the total DWPT load can be expressed as

$$p(t) = \sum_{n=1}^N a_n \sum_{m=-\infty}^{\infty} c_m e^{jm\omega_n(t-t_n)}. \quad (17)$$

Recall that a linear combination of periodic signals is not necessarily periodic. More precisely, signal $p(t)$ is periodic if and only if all ω_n are integer multiples of a single frequency ω_0 . Because this condition is practically impossible, we conclude that $p(t)$ is non-periodic and does not inherit properties p1)–p3) discussed in Section III. Even though $p(t)$ does not have an FS expansion, its frequency-domain analysis is still possible if we can determine its PSD. The following lemma establishes that $p(t)$ is WSS and derives its PSD.

Lemma 4. *Under the assumptions of S4), the total DWPT load $p(t)$ is WSS with mean $\mu_p(t) = N\mu_a c_0$ and PSD*

$$S_p(\omega) = 2\pi(N^2\mu_a^2 + N\sigma_a^2)c_0^2\delta(\omega) + 2\pi N(\mu_a^2 + \sigma_a^2) \sum_{m \neq 0} c_m^2 \phi(\omega; m\mu_\omega, m^2\sigma_\omega^2),$$

where $\phi(x; \mu, \sigma^2)$ denotes the Gaussian probability density function (PDF) with mean μ and variance σ^2 .

Lemma 4 confirms that the PSD of $p(t)$ under S4) is not discrete, but continuous: It consists of Gaussian bells centered around the frequency harmonics $\pm m\mu_\omega$. Consider the m -th Gaussian bell. Because its standard deviation scales with m , its bandwidth is proportional to m and its peak value is inversely proportional to m . Therefore, the Gaussian bells of higher harmonics reduce in amplitude and expand in bandwidth.

If the DWPT spectrum is continuous, we define its THC as:

$$\text{THC}_p = \sqrt{\frac{2 \int_0^\infty S_p(\omega) d\omega}{\lim_{\epsilon \rightarrow 0} \int_{-\epsilon}^\epsilon S_p(\omega) d\omega}} \times 100\%. \quad (18)$$

According to this definition and Lemma 4, the DWPT load has precisely the same THC under S2) and S4). This is because the Gaussian PDF integrates to unity as a function of ω . This observation also implies that the energy contributed by the bell centered around $m\mu_\omega$ under S4) equals the energy of harmonic $m\omega_0$ under S2). Interestingly, scenario S2) can be derived as the limiting case of S4) when σ_v tends to zero and $\mu_v = v$. This originates from the fact that the Dirac delta function is the limiting case of the Gaussian PDF for vanishing variance.

To ease comparison with previous scenarios, consider again deterministic EV densities by setting $\sigma_a = 0$ and $\mu_a = a$. Then, the DC term under S4) scales with Nac_0 and the

Gaussian bell centered around the m -th harmonic scales with $\sqrt{N}a|c_m|$. This is consistent because timings have been assumed independent across EVs as in S2).

Building on the previous lemmas, we next summarize how the THC_p of the DWPT load varies across scenarios.

Corollary 1. *If EVs have identical deterministic densities, the THC_p relates to the THC_h of signal $h_T(t)$ as:*

$$\begin{aligned} \text{THC}_p &= \text{THC}_h && \text{for S1);} \\ \text{THC}_p &= \text{THC}_h/\sqrt{N} && \text{for S2) and S4); and} \\ \text{THC}_p &= \text{THC}_h\sqrt{Q/N} && \text{for S3).} \end{aligned}$$

V. PERIDOGRAMS OF DWPT LOAD DEMANDS

Sections III and IV studied the frequency content of the DWPT load under certain traffic models by deriving its PSD $S_p(\omega)$. The PSD is an *ensemble statistic*. It pertains to all possible realizations of the stochastic load $p(t)$. In practice, however, one would observe a single realization of $p(t)$ at a time. Then, naturally, one asks whether the spectrum of any given realization of $p(t)$ is close enough to $S_p(\omega)$.

This question boils down to whether the *periodogram* of a finite-duration realization of $p(t)$ relates to its PSD. This is a well-studied topic in statistical signal processing [20]. Let us briefly review some key points. Consider a DWPT load realization $\hat{p}(t)$ spanning the finite interval $t \in [0, T_p]$ of duration T_p . Grid operators typically use windows of 1–5 min to compute spectra of signals in power system studies [16]. The periodogram of $\hat{p}(t)$ is computed as the squared magnitude of its Fourier transform as [20, Sec 4.3]

$$\hat{S}_{T_p}(\omega) = \frac{1}{T_p} |\mathcal{F}[\hat{p}(t)]|^2. \quad (19)$$

In addition to the definition in (15), the PSD of $p(t)$ can be defined as the mean of periodograms, asymptotically in T_p :

$$S_p(\omega) = \lim_{T_p \rightarrow \infty} \mathbb{E}[\hat{S}_{T_p}(\omega)] \quad \text{for all } \omega. \quad (20)$$

In plain words, because $\hat{p}(t)$ is random, its periodogram is also random. Each realization $\hat{p}(t)$ yields a different periodogram. The average of periodograms converges to the PSD $S_p(\omega)$ for increasing T_p . Hence, the PSD does not coincide with each periodogram. Instead, it describes the average frequency-domain content of the DWPT load. Intuitively, we expect the periodogram to converge to the PSD for longer windows, higher EV arrival rates, and/or longer highway segments.

In the three tests of this section, we computed numerically the periodograms of 1-min realizations $\hat{p}(t)$, generated according to S2)–S4). More specifically, we simulated the DWPT load consumed by an $L = 16$ km (10 mile)-long ER segment following the specifications of the INDOT ER testbed. EV loads were computed as trapezoidal pulse trains. EV power densities a_n were simulated as iid Gaussian random variables with mean $\mu_a = 94.45$ kW/m and standard deviation $\sigma_a = 5.55$ kW/m; see [22]. For S2) and S3), speed was set to $v = 24.56$ m/s. At this speed, an EV takes about 10 min to cross the ER segment.

Periodogram under S2). To compute the periodogram under S2), EV timings were independently uniformly drawn from

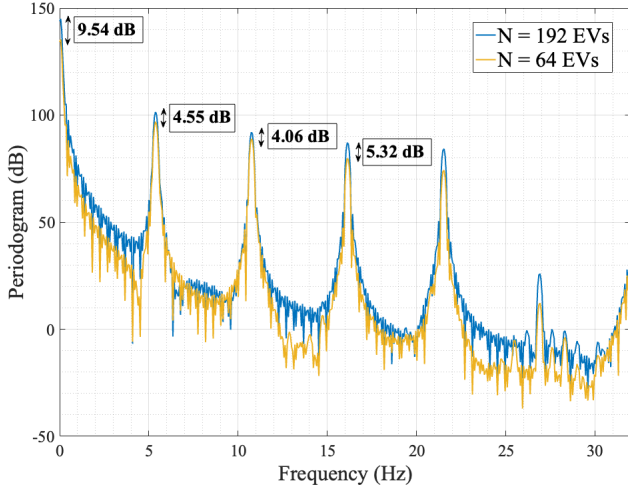


Fig. 3. Periodograms of 1-min DWPT loads simulated under $S2)$ for two values of N . The magnitude and location of harmonics agree with those predicted by Lemma 2. Moreover, as asserted by Lemma 2, the ratio of the two periodograms should be $10 \log_{10} (192/64)^2 = 9.54$ dB at DC, and about $10 \log_{10} (192/64) = 4.77$ dB at harmonic components.

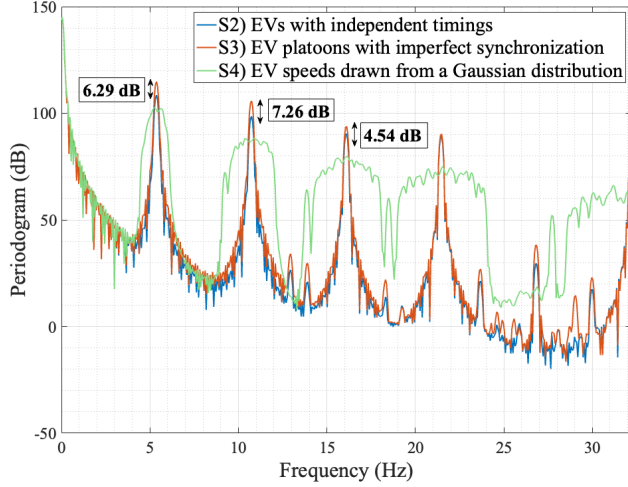


Fig. 4. Periodograms of 1-min DWPT loads simulated under $S2)$ – $S4)$ for $N = 192$ EVs. Harmonics increase in power under $S3)$ due to platoons. The increase is about $10 \log_{10} Q = 6.98$ dB per Lemmas 2–3. The bells under $S4)$ are centered around the harmonics of $S2)$ because $\mu_v = 55$ mph. Bells reduce in magnitude and spread in bandwidth with m per Lemma 4.

$[0, T)$, where $T = D/v$. Because independent timings are likely to occur under lighter traffic, we considered two relatively low values of the mean arrival rate λ_a , namely 0.1 and 0.3 EV/s, yielding $N = 64$ and 192 EVs, respectively. Figure 3 depicts the periodogram of a single 1-min realization of $\hat{p}(t)$ after applying a Hanning window. This periodogram differs from the PSD of Lemma 2 as it relies on a single, finite-duration realization $\hat{p}(t)$. Nonetheless, the locations of harmonic peaks coincide with those predicted by the analysis. For $N = 64$ and $N = 192$, the DC component of $\hat{p}(t)$ was 8.70 MW and 26.13 MW, respectively. Integrating the two periodograms around the first harmonic yielded 357 kW and 680 kW, respectively, for the two values of N . This verifies that although the DC component scales with N , harmonics scale with \sqrt{N} . In addition, we evaluated the THC for multiple realizations $\hat{p}(t)$ and found it to be 3–6% and 1–3% for the two values of N , indicating that the THC decreases with N .

Periodogram under $S3)$. In this case, we simulated $N = 192$ EVs moving in platoons of approximately $Q = 5$ EVs per platoon. To capture imperfect synchronization, we first sampled the timing of each platoon independently uniformly from $[0, T)$. Then, for each EV within a platoon, we added an extra time shift drawn independently uniformly from $[0, T/5]$. Figure 4 illustrates the obtained periodogram. Although EVs within a platoon are not perfectly synchronized, the obtained spectrum contains higher harmonic content compared to the spectrum under $S2)$. As dictated by Lemmas 2 and 3, although the DC components are identical (barring the deviations of a single periodogram from its mean), harmonics do increase in power under $S3)$, as they now scale as \sqrt{QN} instead of \sqrt{N} . In addition, we computed the THC under different realizations and found it to be around 3% under imperfect synchronization and 16% under perfect synchronization within platoons.

Periodogram under $S4)$. To simulate $S4)$, EV speeds v_n were drawn independently from a Gaussian PDF with $\mu_v = 24.56$ m/s (55 mph) and $\sigma_v = 1.23$ m/s (2.75 mph), while EV timings t_n were iid and uniform in $[0, D/v_n)$. Figure 4 compares the periodograms obtained under $S4)$ to $S2)$ and $S3)$ for $N = 192$ EVs. Unequal speeds cause spectrum spreading under $S4)$. As asserted by Lemma 4, the bandwidth of the bells increases with m . The magnitude of the peaks is smaller under $S4)$ rather than $S2)$, as expected. The test also corroborates that the THCs for $S2)$ and $S4)$ are equal on average.

VI. TESTS USING THE SUMO SIMULATOR

To better understand the spectra of real-world traffic, we simulated DWPT loads with the help of SUMO [23], an open-source microscopic traffic flow simulator. It can generate realistic trajectories of vehicles driving over a roadway under different specified conditions. Given the trajectory of each EV $_n$, its load $p_n(t)$ can be computed using (3) and (4). The demand $p(t)$ is computed as the sum of EV loads.

We simulated an $L = 4$ km (2.5 mile) ER segment with two lanes; the rightmost one is the DWPT lane. Vehicles were allowed to change lanes. All vehicles driving in the DWPT lane were considered to be EVs of the same type (class-8 trucks). The DWPT parameters (ℓ_T, ℓ_R, d) matched the INDOT testbed specifications. EV power densities were drawn independently from a Gaussian distribution with mean $\mu_a = 94.45$ kW/m and standard deviation $\sigma_a = 5.55$ kW/m. For SUMO parameters, we set the maximum vehicle speed to be 36 m/s (80 mph), while vehicle acceleration was constrained to lie within $[-4.5, 2.6]$ m/s 2 . Successive vehicles were spaced by more than 2.5 m and 1 sec. Traffic followed the Krauss car-following model [24]. According to this model, the driver of vehicle n has a *desired speed* v_n^d , but may have to slow down depending on the speed of the leading vehicle.

Free-flowing traffic conditions. With our first test using SUMO, we wanted to test whether $S4)$ can explain the spectrum of the DWPT load under light traffic. To this end, we simulated a mean arrival rate of $\lambda_a = 0.21$ EV/s. The desired EV speeds v_n^d were drawn from a truncated Gaussian distribution with mean $\mu_v = 24.56$ m/s, standard deviation $\sigma_v = 2.45$ m/s (5.5 mph), while the lower and upper cutoff

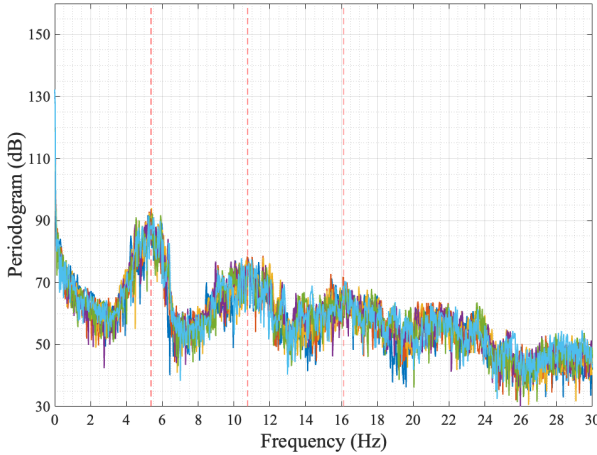


Fig. 5. Periodograms computed using 1-min DWPT loads simulated using SUMO under light traffic conditions. The periodograms contain bells centered around harmonics of $f_0 = 5.38$ Hz associated with mean speed $\mu_v = 24.56$ m/s (55 mph) and the INDOT tested segment spacing. Bells decay in magnitude and spread in bandwidth with increasing m , as asserted by Lemma 4. Periodograms across realizations are similar in shape.

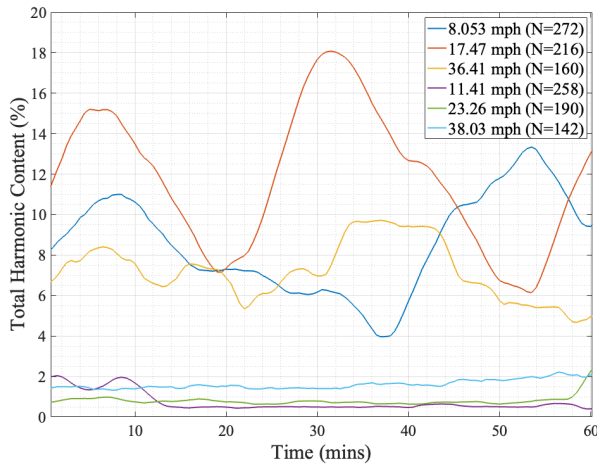


Fig. 6. Variation of THC across time under low-speed, high-volume traffic simulated in SUMO. The speed affects the number of EVs and the EV spacing. Some speeds result in near-synchronization and high THC, as in *S1*), and other speeds result in lower THC, as in *S4*).

speeds were set to 20.11 m/s (45 mph) and 29.05 m/s (65 mph), respectively. We simulated traffic for over 40 min, and then randomly selected 1-min intervals as $\hat{p}(t)$. The total number of EVs driving on the ER segment remained relatively constant at $N = 49$ EVs across all 1-min intervals; see Remark 2. Figure 5 depicts the periodograms obtained over 6 Monte Carlo runs. The DC component is 6.8 MW, the power contained around the first harmonic is 613.70 kW. THC in the range of 6–7% was observed for different $\hat{p}(t)$ segments. Overall, the key features of the spectra in Fig. 5 agree with the analysis under *S4*).

Congested traffic conditions. With the next test, we wanted to see if there exist traffic conditions under which the DWPT demand exhibits higher THC due to EV synchronization as in *S1*). To this end, we studied the DWPT load on an ER with heavy traffic moving at a slower speed. Such conditions can arise due to an accident, adverse weather conditions, or construction activities. To simulate such traffic conditions in SUMO, the speed limit was 24.56 m/s (55 mph) on the first half of the ER and lowered on the second part.

Initial EV speeds were drawn from the truncated Gaussian distribution explained earlier. The mean arrival rate was set to $\lambda_a = 1$ EV/s. At this rate, the traffic jam propagated from the second half backwards to the beginning of the ER. Eventually, all EVs were moving at roughly the slower speed limit of the second half. Inter-vehicle spacings were found to be approximately constant across vehicles and time.

As explained under *S1*), EV loads at constant speed can synchronize only when EV spacings are integer multiples of the coil segment length D . Moreover, the distance gap between EVs increases with the speed limit [24]. Based on this understanding, we identified several speed limits for the second half of the ER, at which approximate synchronization occurs and leads to high THC. Figure 6 depicts how the THC of the total DWPT load demand evolves across time for different jam speeds. The THC was computed based on 1-min segments of $p(t)$ with a 50% overlap. We observe that higher speeds result in fewer EVs, as expected based on Remark 2. We also note that the THC scales as THC_h/\sqrt{N} for the bottom three speed limits, for which the inter-vehicle distance was not a multiple of D . On the contrary, for the top three speed limits, THC increases due to the resonance of traffic with the ER infrastructure. The maximum THC value we observed was 18% for a particular 1-minute segment when the jam moves at 7.81 m/s (17.47 mph). Overall, this experiment validates the conjecture made in *S1*) that the DWPT load demand can exhibit high THC under heavy traffic conditions moving at specific speeds, especially at relatively lower speed limits. Also, the THC appears to be varying sinusoidally, which is a common phenomenon for frequency-modulated signals [20]. Analyzing the PSD under time-varying velocities and a detailed explanation of this sinusoidal variation in THC would be the topic of future study.

VII. CONCLUSIONS

This work puts forth statistical models for the total load to be consumed at the substation serving an ER. By postulating different distributions on EV timings, our analysis explains how the DWPT load spectrum varies under various traffic conditions. The worst-case scenario in terms of THC occurs when EVs move in a synchronized fashion with particular EV spacings. Simulations using SUMO demonstrate that near synchronization can occur under low-speed, high-volume traffic. When EVs move freely, the DWPT load exhibits a more favorable spectrum profile, as verified by simulating low-volume traffic in SUMO. Frequency content at non-DC frequencies scales with \sqrt{N} or N depending on EV synchronism. Platoon formations can yield higher THC. In general, the fundamental frequency depends on the spacing between coils and the average EV speed, so that low-speed traffic can result in harmonics below 2 Hz. Higher-order harmonics decrease in magnitude and spread across a wider bandwidth. Despite the simplicity of the models, our findings provide valuable insights to ER planners and grid operators on how the DWPT spectrum scales with the number of EVs. This work can be expanded in various directions: *a*) Model DWPT load when EVs move with time-varying speeds using tools from frequency-modulated

signals; b) Study the effect of correlated EV speeds based on dynamical models of traffic flows; c) Analyze the effect of DWPT load consumed at multiple buses on grid frequency dynamics; and d) Develop solutions to smooth out DWPT load.

VIII. APPENDIX

Proof of Lemma 1: According to (12)–(13), the squared THC of $p(t)$ can be expressed as

$$\text{THC}_p^2 = \frac{2 \sum_{m=1}^{\infty} |\tilde{c}_m|^2}{\tilde{c}_0^2} = 2 \sum_{m=1}^{\infty} \frac{|\tilde{c}_m|^2}{\tilde{c}_0^2}. \quad (21)$$

We would like to maximize THC_p^2 over the EV parameters $\{a_n, t_n\}_{n=1}^N$, collected in vectors \mathbf{a} and \mathbf{t} , respectively. Define vector $\mathbf{b}_m(\mathbf{t}) \in \mathbb{C}^N$ so its n -th entry is $e^{-jm\omega_0 t_n}$ for all $m \geq 0$. We can then express $|\tilde{c}_m|^2$ in (21) as

$$|\tilde{c}_m|^2 = |c_m|^2 \cdot |\mathbf{a}^\top \mathbf{b}_m(\mathbf{t})|^2.$$

Note that $\mathbf{b}_0(\mathbf{t}) = \mathbf{1}$ for any \mathbf{t} , where $\mathbf{1}$ is the all-one vector. For any $m \geq 1$, consider maximizing the ratio over (\mathbf{a}, \mathbf{t}) :

$$\frac{|\tilde{c}_m|^2}{\tilde{c}_0^2} = \frac{|c_m|^2 |\mathbf{a}^\top \mathbf{b}_m(\mathbf{t})|^2}{c_0^2 |\mathbf{a}^\top \mathbf{1}|^2} \leq \frac{|c_m|^2 \|\mathbf{a}\|_1^2 \|\mathbf{b}_m(\mathbf{t})\|_\infty^2}{c_0^2 \|\mathbf{a}\|_1^2} = \frac{|c_m|^2}{c_0^2}$$

due to Hölder's inequality and $\|\mathbf{b}_m(\mathbf{t})\|_\infty = 1$ for any \mathbf{t} .

Consider now some particular choices of \mathbf{t} . Suppose all EVs have equal timings, so that $\mathbf{t} = t_0 \mathbf{1}$ for some $t_0 \in [0, T)$. For this \mathbf{t} , it holds that $|\mathbf{a}^\top \mathbf{b}_m(\mathbf{t})| = |\mathbf{a}^\top \mathbf{1}| = \|\mathbf{a}\|_1 \cdot \|\mathbf{b}_m(\mathbf{t})\|_\infty$, so the ratio $|\tilde{c}_m|/\tilde{c}_0$ attains its upper bound regardless of the value of \mathbf{a} . Clearly, the choice of $\mathbf{t} = t_0 \mathbf{1}$ maximizes THC_p^2 in (21). The maximum value is $\text{THC}_p = \text{THC}_h$. ■

Proof of Lemma 2: First, apply the expectation operator on (11) to find the mean of $p_n(t)$ as

$$\begin{aligned} \mathbb{E}[p_n(t)] &= \mathbb{E} \left[a_n \sum_{m=-\infty}^{\infty} c_m e^{jm\omega_0 t} e^{-jm\omega_0 t_n} \right] \\ &= \mathbb{E}[a_n] \sum_{m=-\infty}^{\infty} c_m e^{jm\omega_0 t} \cdot \mathbb{E}[e^{-jm\omega_0 t_n}] \\ &= \mu_a \sum_{m=-\infty}^{\infty} c_m e^{jm\omega_0 t} \delta[m] = \mu_a c_0 \end{aligned} \quad (22)$$

where $\delta[m]$ is Kronecker delta function. The third equality holds due to t_n being uniform in $[0, T)$ with $T = \frac{2\pi}{\omega_0}$ so that:

$$\mathbb{E}[e^{-jm\omega_0 t_n}] = \frac{1}{T} \int_0^T e^{-jm\omega_0 t_n} dt_n = \delta[m].$$

The mean can be computed as $\mathbb{E}[p(t)] = \sum_{n=1}^N \mathbb{E}[p_n(t)] = N\mu_a c_0$. The autocorrelation function of $p(t)$ can be found as

$$\begin{aligned} \mathbb{E}[p(t)p(t+\tau)] &= \sum_{n=1}^N \sum_{\ell=1}^N \mathbb{E}[p_n(t)p_\ell(t+\tau)] \\ &= R_a(\tau) + R_c(\tau) \end{aligned} \quad (23)$$

The double summation involves N terms with $\ell = n$ contained in $R_a(\tau)$, and $N(N-1)$ terms with $\ell \neq n$ contained in $R_c(\tau)$. We expound on these two terms, starting with the first one:

$$R_a(\tau) = \sum_{n=1}^N \sum_{\ell=n}^N \mathbb{E}[p_n(t)p_n(t+\tau)]$$

$$= N\mathbb{E}[p_n(t)p_n(t+\tau)] = NR_n(\tau).$$

The autocorrelation of $p_n(t)$ can be computed as

$$\begin{aligned} R_n(\tau) &= \mathbb{E}[a_n^2] \sum_m \sum_k c_m c_k e^{jm\omega_0 t} e^{jk\omega_0(t+\tau)} \mathbb{E}[e^{-j(m+k)\omega_0 t_n}] \\ &= (\mu_a^2 + \sigma_a^2) \sum_m \sum_k c_m c_k e^{j(m+k)\omega_0 t} e^{jk\omega_0 \tau} \delta[m+k] \\ &= (\mu_a^2 + \sigma_a^2) \sum_m c_m c_{-m} e^{-jm\omega_0 \tau} \\ &= (\mu_a^2 + \sigma_a^2) \sum_{m=-\infty}^{\infty} c_m^2 e^{-jm\omega_0 \tau} \\ &= (\mu_a^2 + \sigma_a^2) \left(c_0^2 + 2 \sum_{m=1}^{\infty} c_m^2 \cos(m\omega_0 \tau) \right). \end{aligned}$$

Since the loads $p_n(t)$ are uncorrelated, the term $R_c(\tau)$ is

$$\begin{aligned} R_c(\tau) &= \sum_{n=1}^N \sum_{\ell \neq n}^N \mathbb{E}[p_n(t)p_\ell(t+\tau)] \\ &= \sum_{n=1}^N \sum_{\ell \neq n}^N \mathbb{E}[p_n(t)] \cdot \mathbb{E}[p_\ell(t+\tau)] \\ &= N(N-1)\mu_a^2 c_0^2, \end{aligned}$$

where the third equality follows from (22). Adding $R_a(\tau)$ and $R_c(\tau)$, and collecting the terms related to the DC term provides the final expression for the autocorrelation of $p(t)$:

$$R_p(\tau) = (N^2 \mu_a^2 + N \sigma_a^2) c_0^2 + 2N(\mu_a^2 + \sigma_a^2) \sum_{m=1}^{\infty} c_m^2 \cos(m\omega_0 \tau).$$

The signal $p(t)$ is WSS because its mean is time-invariant and its autocorrelation depends only on τ . Its PSD $S_p(\omega)$ can be found as the Fourier transform of $R_p(\tau)$. ■

Proof of Lemma 3: We index platoons by $i = \{1, \dots, N/Q\}$. Let the EVs belonging to platoon i constitute the set \mathcal{N}_i and share timing t_i , which is drawn uniformly at random within $[0, T)$. The total load can be decomposed as

$$\begin{aligned} p(t) &= \sum_{i=1}^{N/Q} \sum_{n \in \mathcal{N}_i} p_n(t) = \sum_{i=1}^{N/Q} \left(\sum_{n \in \mathcal{N}_i} a_n \right) \sum_m c_m e^{jm\omega_0(t-t_i)} \\ &= \sum_{i=1}^{N/Q} a_i \sum_m c_m e^{jm\omega_0(t-t_i)} \end{aligned}$$

where a_i is defined as the effective rating of platoon i . Based on this decomposition, the DWPT load is now amenable to the analysis of Lemma 2 subject to two modifications. First, signal $p(t)$ is now the sum of N/Q rather than N stochastic components, each with iid and uniformly distributed timings t_i . Second, the effective rating a_i of each stochastic component has a mean $Q\mu_a$ and its variance is increased to $Q\sigma_a^2$. The mean and autocorrelation of $p(t)$ can be obtained as in Lemma 2 by simply replacing N by N/Q , μ_a by $Q\mu_a$, and σ_a^2 by $Q\sigma_a^2$. The autocorrelation function is

$$\begin{aligned} R_p(\tau) &= (N^2 \mu_a^2 + N \sigma_a^2) c_0^2 \\ &\quad + 2(N^2 \mu_a^2 + N \sigma_a^2) \sum_{m=1}^{\infty} c_m^2 \cos(m\omega_0 \tau). \end{aligned}$$

The PSD can be found as the Fourier transform of $R_p(\tau)$. ■

Proof of Lemma 4: This proof builds on the proof of Lemma 2. Applying the expectation operator on (17) yields

$$\begin{aligned}\mathbb{E}[p(t)] &= \sum_{n=1}^N \mathbb{E}[a_n] \sum_{m=-\infty}^{\infty} c_m \mathbb{E}[e^{jm\omega_n(t-t_n)}] \\ &= \sum_{n=1}^N \mu_a \sum_{m=-\infty}^{\infty} c_m \delta[m] = N\mu_a c_0.\end{aligned}$$

The second equality stems from the law of total expectation, according to which [20]

$$\begin{aligned}\mathbb{E}[e^{jm\omega_n(t-t_n)}] &= \mathbb{E}_{\omega_n} [\mathbb{E}_{t_n} [e^{jm\omega_n(t-t_n)} | \omega_n]] \\ &= \mathbb{E}_{\omega_n} [e^{jm\omega_n t} \mathbb{E}_{t_n} [e^{-jm\omega_n t_n} | \omega_n]] \\ &= \mathbb{E}_{\omega_n} [e^{jm\omega_n t} \delta[m]] = \delta[m]\end{aligned}$$

Regarding the autocorrelation function, we follow the steps of Lemma 2 and decompose $R_p(\tau)$ as [cf. (23)]

$$R_p(\tau) = R_a(\tau) + R_c(\tau) = NR_n(\tau) + N(N-1)\mu_a^2 c_0^2.$$

To find $R_p(\tau)$, it suffices to find the autocorrelation function $R_n(\tau)$ of $p_n(t)$ as follows:

$$\begin{aligned}R_n(\tau) &= \mathbb{E}[a_n^2] \sum_{m,k} c_m c_k \mathbb{E} [e^{jm\omega_n(t-t_n)} e^{jk\omega_n(t-t_n)} e^{jk\omega_n \tau}] \\ &= \mathbb{E}[a_n^2] \sum_{m,k} c_m c_k \mathbb{E}_{\omega_n} [e^{j(m+k)\omega_n t} e^{jk\omega_n \tau} \mathbb{E}_{t_n} [e^{-j(m+k)\omega_n t_n}]] \\ &= (\mu_a^2 + \sigma_a^2) \sum_{m,k} c_m c_k \mathbb{E}_{\omega_n} [e^{j(m+k)\omega_n t} e^{jk\omega_n \tau} \delta[m+k]] \\ &= (\mu_a^2 + \sigma_a^2) \sum_m c_m c_{-m} \mathbb{E}_{\omega_n} [e^{-jm\omega_n \tau}] \\ &= (\mu_a^2 + \sigma_a^2) \sum_m c_m^2 e^{-jm\mu_\omega \tau} e^{-\frac{1}{2}m^2\sigma_\omega^2 \tau^2}.\end{aligned}$$

The last equality follows from the characteristic function of the Gaussian distribution. In detail, for a Gaussian distributed random variable $x \sim \mathcal{N}(\mu_x, \sigma_x^2)$, its characteristic function can be shown to be [20]

$$\Phi_x(z) = \mathbb{E}[e^{jxz}] = e^{jz\mu_x} e^{-\frac{1}{2}z^2\sigma_x^2}.$$

Substituting $R_n(\tau)$ into $R_p(\tau)$ and separating the component related to c_0^2 provides the final expression for $R_p(\tau)$:

$$\begin{aligned}R_p(\tau) &= (N^2\mu_a^2 + N\sigma_a^2)c_0^2 \\ &\quad + N(\mu_a^2 + \sigma_a^2) \sum_{m \neq 0} c_m^2 e^{-jm\mu_\omega \tau} e^{-\frac{1}{2}m^2\sigma_\omega^2 \tau^2}.\end{aligned}$$

The PSD of $p(t)$ is the Fourier transform of $R_p(\tau)$. The Fourier transform of the constant term related to $m = 0$ in $R_p(\tau)$ yields the $\delta(\omega)$ term in $S_p(\omega)$. Let us compute the Fourier transform of the terms related to $m \neq 0$ in $R_p(\tau)$. To this end, we evaluate the next integral as

$$\int_{-\infty}^{\infty} e^{-jm\mu_\omega \tau} e^{-\frac{1}{2}m^2\sigma_\omega^2 \tau^2} e^{-j\omega \tau} d\tau = \frac{\sqrt{2\pi}}{m\sigma_\omega} e^{-\frac{1}{2}m^2\sigma_\omega^2 \tau^2}.$$

This identity follows if we consider $\tau \sim \mathcal{N}(0, \frac{1}{m^2\sigma_\omega^2})$ and evaluate its characteristic function $\Phi_\tau(z)$ at $z = -(\omega + m\mu_\omega)$. ■

REFERENCES

- [1] D. Haddad, T. Konstantinou, A. Prasad *et al.*, "Data-driven design and assessment of dynamic wireless charging systems," in *IEEE PELS Workshop on Emerging Technologies: Wireless Power Transfer*, London, UK, Jun. 2019, pp. 59–64.
- [2] D. Haddad, T. Konstantinou, D. Aliprantis *et al.*, "Analysis of the financial viability of high-powered electric roadways: A case study for the state of Indiana," *Energy Policy*, vol. 171, p. 113275, Dec. 2022.
- [3] X. Zhu, B. Mather, and P. Mishra, "Grid impact analysis of heavy-duty electric vehicle charging stations," in *Proc. IEEE Conf. on Innovative Smart Grid Technologies*, Washington, DC, Feb. 2020, pp. 1–5.
- [4] R. El Helou, S. Sivaranjani, D. Kalathil *et al.*, "The impact of heavy-duty vehicle electrification on large power grids: A synthetic Texas case study," *Advances in Applied Energy*, vol. 6, p. 100093, Jun. 2022.
- [5] V. Mehar, N. Frooninckx, I. Abram *et al.*, "Receiver-side power control of a 200-kW three-phase DWPT system for heavy-duty vehicles," in *Proc. Wireless Power Tech. Conf. and Expo*, Rome, Italy, Jun. 2025.
- [6] A. Sauter, J. D. Lara, J. Turk *et al.*, "Power system operational impacts of electric vehicle dynamic wireless charging," *Applied Energy*, vol. 364, p. 123002, Jun. 2024.
- [7] H. Xie, T. Ding, S. Liu *et al.*, "Sequential power flow simulation of integrated dynamic wireless power transfer systems," in *Proc. IEEE PES General Meeting*, Boston, MA, Jul. 2016, pp. 1–5.
- [8] T. M. Newbolt, P. Mandal, H. Wang *et al.*, "Diverse effects of dynamic wireless power transfer roadway in-motion electric vehicle charging," in *Proc. IEEE Conf. on Innovative Smart Grid Technologies*, Washington, DC, Jan. 2023, pp. 1–5.
- [9] W. Liu, X. Wang, and Y. Xu, "Bilevel planning of wireless charging lanes in coupled transportation and power distribution networks," *IEEE Trans. Transp. Electrification*, vol. 10, no. 2, pp. 2499–2510, Jul. 2023.
- [10] T. Newbolt, P. Mandal, H. Wang *et al.*, "Feasibility of dynamic wireless power transfer to mitigate load demands under resiliency events," in *Proc. IEEE PES General Meeting*, Austin, TX, Jul. 2024, pp. 1–5.
- [11] A. Gupta, M. K. Singh, and V. Kekatos, "Incorporating power system stability metrics into the optimal power flow," in *Proc. IEEE American Control Conf.*, Denver, CO, Jul. 2025.
- [12] C. Batlle, M. Barruso, and P. Rodilla, "The (hopefully) enlightening blackout in Spain: Questions and lessons for the future," MIT Center for Energy and Environmental Policy Research, Tech. Rep., Jul. 2025.
- [13] Y. Cheng, L. Fan, J. Rose *et al.*, "Real-world subsynchronous oscillation events in power grids with high penetrations of inverter-based resources," *IEEE Trans. Power Syst.*, vol. 38, no. 1, pp. 316–330, Jan. 2023.
- [14] M. Alizadeh and X. Wang, "Root cause analysis of frequency oscillations observed in Ontario's distribution system," *IEEE Trans. Power Syst.*, pp. 1–12, 2025.
- [15] J. Lian, S. Wang, M. A. Elizondo *et al.*, "Universal wide-area damping control for mitigating inter-area oscillations in power systems," Pacific Northwest National Lab, Richland, WA, Tech. Rep., 2017.
- [16] C. Mishra, L. Vanfretti, J. Delaree Jr *et al.*, "Understanding the inception of 14.7 Hz oscillations emerging from a data center," *Sustainable Energy, Grids and Networks*, p. 101735, May 2025.
- [17] T. Newbolt, P. Mandal, H. Wang *et al.*, "Sustainability of dynamic wireless power transfer roadway for in-motion electric vehicle charging," *IEEE Trans. Transp. Electrification*, vol. 10, no. 1, pp. 1347–1362, Mar. 2023.
- [18] S. Bafandkar and A. Talebpour, "Charging while driving lanes: A boon to electric vehicle owners or a disruption to traffic flow," *arXiv preprint arXiv:2504.14360*, 2025.
- [19] T. Newbolt, M. Waite, P. Mandal *et al.*, "Load demand modeling of large-scale charging infrastructure for electric vehicles in-motion," *IEEE Access*, Nov. 2024.
- [20] J. G. Proakis, M. Salehi, N. Zhou *et al.*, *Communication systems engineering*, 2nd ed. Upper Saddle River, NJ: Prentice-Hall, 1994.
- [21] S. M. Ross, *Introduction to Probability Models*, 10th ed. San Diego, CA: Academic Press, 2007.
- [22] A. D. Brovont, D. Aliprantis, S. D. Pekarek *et al.*, "Design and analysis of a three-phase dynamic wireless power transfer system for heavy-duty electric vehicles considering misalignment," in *Proc. Wireless Power Week*, Bordeaux, France, Jul. 2022, pp. 867–872.
- [23] P. A. Lopez, M. Behrisch, L. Bieker-Walz *et al.*, "Microscopic traffic simulation using SUMO," in *Proc. Intl. Conference on Intelligent Transportation Systems*, Maui, HI, Nov. 2018, pp. 2575–2582.
- [24] S. Krauß, "Microscopic modeling of traffic flow: Investigation of collision free vehicle dynamics," Ph.D. dissertation, University of Cologne, 1998.